



Research article

Health assessment of an electro-hydraulic servo pump control system for servomotor based on LGA deep neural network

Fei Wang^{a,b}, Gexin Chen^{a,b,*}, Keyi Liu^b, Tiangui Zhang^a, Yuan Li^a, Chao Ai^a^a School of Mechanical Engineering, Yanshan University, Qinhuangdao 066004, China^b Mechanical and Electrical Engineering, Xinjiang Institute of Engineering, Urumqi 830023, China

ARTICLE INFO

Keywords:

Servomotor
EHSPCS
LGA deep neural network
Health assessment
Feature parameter extraction

ABSTRACT

Due to its advantages of having a high power-to-weight ratio and being energy-efficient, the electro-hydraulic servo pump control system (abbreviated as EHSPCS) is frequently employed in the industrial field, such as the electro-hydraulic servo pump control (EHSPC) servomotor for steam turbine valve regulation control. However, the EHSPCS has strong nonlinearity and time-varying features, and the factors that cause system performance degradation are complex. Once a system failure occurs, it may lead to serious accidents, causing serious casualties and economic losses. To address the above issues, a system health assessment method based on LSTM-GRNN-ANN (LGA) deep neural network is proposed in this paper. Firstly, with oil volume gas content, servo motor air-gap flux density, and system leakage coefficient as the health assessment performance indicators, a health assessment performance index system for the EHSPCS is built. Furthermore, the system performance index threshold is set. Secondly, an LGA deep neural network is constructed by combining LSTM, GRNN and ANN, and a deep neural network based on the LGA is used to create an EHSPCS health assessment model. Subsequently, system feature parameter extraction, algorithm design, and parameter debugging are carried out. Finally, an EHSPCS experimental platform is established, typical system failure simulation experiments are designed, and comparative experimental analysis is conducted. The experimental findings demonstrate that the average accuracy of the system health assessment model based on the LGA deep neural network suggested in this paper is 96.37%, compared to 89.84%, 87.99% for LSTM and GRNN, which validates the accuracy of the system health assessment model based on the LGA deep neural network.

1. Introduction

The power industry's most used primary mover device is the steam turbine. Being a crucial component of the steam turbine unit, the hydraulic servomotor modifies the high-pressure steam intake volume by altering the inlet valve, hence regulating the system power and being crucial to the unit's performance [1]. A volume servo integrated powertrain, which offers the benefits of a high power-to-weight ratio, short response time, good control performance and low cost, is adopted by an EHSPCS [2], and is widely used in aerospace [3], wind power [4], vessel [5], engineering machinery [6] and other fields. In recent years, with the continuous breakthroughs in servo motor technology, the EHSPCS's control precision and reaction time have been greatly improved. The working time

* Corresponding author. School of Mechanical Engineering, Yanshan University, Qinhuangdao 066004, China.
E-mail address: jygxchen@ysu.edu.cn (G. Chen).

<https://doi.org/10.1016/j.heliyon.2024.e26936>

Received 15 August 2023; Received in revised form 19 February 2024; Accepted 21 February 2024

Available online 28 February 2024

2405-8440/© 2024 The Authors. Published by Elsevier Ltd. This is an open access article under the CC BY-NC-ND license (<http://creativecommons.org/licenses/by-nc-nd/4.0/>).

in complex and harsh environments has become longer and longer, and the requirements for performance and safety have also become higher [7]. This has led to more and more technicians and enterprises researching and promoting the use of EHSPC technology [8,9]. However, the EHSPCS multiple subsystems such as mechanical, electronic, hydraulic, and control, with strong nonlinearity and time-varying characteristics. Under internal and external disturbances of the system, there are motor torque fluctuations, quantitative pump pressure pulsation, and system leakage. In addition, coupled with complex failure mechanisms and other unknown factors, the system is easy to appear degradation and failures [10]. In order to prevent serious consequences caused by the degradation or failure of the system's health status, operators must timely acquire the operating status of mechanical equipment. Therefore, it is particularly important to quickly and accurately assess the system's health state.

In the 1970s, the United States had already proposed the concept of the integrated vehicle health management (IVHM) in the aerospace field, aiming to build a comprehensive management system for real-time analysis and processing of aircraft health state [11]. With the continuous development and optimization of information processing and artificial intelligence methods, researchers have also achieved new breakthroughs in the health assessment methods of electro-hydraulic servo systems. Kim [12] applied wireless sensors for status monitoring in system maintenance and management, and developed a method for extracting data features using the Boruta algorithm, which achieved stability assessment of the hydraulic system's various components' current operational state. Kosova [13] presented a feature extraction method based on linear discriminant analysis (LDA) to reduce the dimension of features. Macaluso [14] proposed a PHM health assessment system based on critical factor analysis and detection (FMECA), which enabled accurate assessment of system status with fewer sensors. Duan [15] presented a fuzzy comprehensive evaluation (FCE) health assessment method based on enhanced risk coefficient optimization, which reduced subjective judgment errors caused by expert experience and improved the accuracy of health assessment. Mei [16] proposed a method that combines the cloud models with the Dempster Shafer evidence theory and achieved health status assessment of complex hydraulic systems.

Based on the strong adaptability, self-learning and nonlinear mapping capabilities of neural network, different types of neural network were also widely employed in the health assessment research of the electro-hydraulic servo systems. Gareev [17] proposed a neural network health assessment method based on gated convolutional autoencoder, which achieved accurate recognition of hydraulic system status in a short period of time, with an average assessment accuracy of over 99%. In order to determine the state value boundary of the power system, Lu [18] established a new ISF based game, proposed ensemble learning of LSTM to obtain predicted states, and used parameter Gaussian distribution to describe the uncertainty of the states. Chen [19] proposed a new two-layer nonlinear combination method, EELELM, which utilizes long short term memory neural network (LSTM), elman neural network (ENN), and extreme learning machine (ELM) to respectively predict wind speed. Simulation results show that higher accuracy levels can be achieved. Keleko [20] proposed a condition monitoring (CM) method based on the DNN and multi-sensor data, which improved the system health assessment model's robustness. Song [21] proposed a system health assessment model of hydraulic on the basis of the GRNN, established an adaptive health baseline assessment system, and achieved the switching of assessment models and adaptive threshold adjustment under different working conditions. Nie [22] developed a real-time thermal network modified models innovatively using artificial neural networks, which uses trained models and online data to calibrate parameters and analog the deterioration of online EHA performance, for the health management (PHM) and prognosis (PH) of EHA in real-world operating circumstances.

In summary, scholars had made many key advances and technological achievements in the health assessment of electro-hydraulic servo systems. However, there is relatively little research on the health assessment of the EHSPCS, and there is no public literature published in the field of the EHSPC servomotor. The application of neural network also extracts features separately from temporal or spatial dimensions, which has certain limitations. At the same time, there has been no research on deep aggregation of LSTM, GRNN, and ANN (BP) neural networks. Therefore, based on the analysis of performance indicators for health assessment of the EHSPCS, this article proposes an LSTM-GRNN-ANN (LGA) deep neural network health assessment method that integrates LSTM, GRNN, and ANN (BP). This method captures the mutual influence relationship between system parameters from both time and space dimensions, which can further improve the accuracy of health assessment, provide theoretical support for the health assessment research of EHSPCS.

The main innovations of this article are as follows:

- 1) On the basis of theoretical analysis, performance indicators such as oil gas content, servo motor air-gap flux density, and system leakage coefficient are proposed innovatively. Moreover, an EHSPCS health assessment performance index system is established, and the performance index threshold of the system is further set.
- 2) Taking advantage of the fast computation speed or strong ability in forecasting of LSTM, GRNN, and ANN (BP), an LSTM-GRNN-ANN (LGA) deep neural network health assessment method combining LSTM, GRNN, and ANN (BP) is proposed. This method extracts feature parameters from both temporal and spatial dimensions and handles the interrelationships between parameters. Finally, an EHSPCS health assessment model is established based on this method for the health assessment of the EHSPCS.

2. Principle and mathematical modeling of the EHSPCS for servomotor

2.1. Servo motor model

The EHSPCS researched in this article is divides into three parts: hydraulic, electrical and mechanical. The hydraulic part consists of a servo motor, an axial quantitative piston pump, an accumulator, two one-way valves, two relief valves, a cylinder, and hydraulic accessories. The EHSPCS adopts the principle of volume control. The servo motor drives the axial quantitative piston pump coaxial; The discharge and suction ports of the pump are directly connected to the low and high pressure load chambers of the cylinder; The

accumulator connects the low-pressure chamber of the system to replenish oil to the system through the one-way valve; The relief valve provides pressure overload protection for the system; The cylinder changes the high-pressure steam intake air of the turbine by adjusting the opening of the inlet valve. The system composition and working principle is shown in Fig. 1.

2.2. Mathematics modeling of the EHSPCS

2.2.1. Servo motor model

This article adopts a servo motor vector control method based on rotor magnetic field orientation. When the EHSPCS reaches steady state, the servo motor model can be shown as Eq. (1):

$$\begin{cases} T_c = \frac{3}{2}\varphi_f P_n i_q \\ U_q = L_q \dot{i}_q + R_s i_q + K_e \omega_e \\ T_c - T_L = J_L \dot{\omega}_m + B_m \omega_m \end{cases} \quad (1)$$

where T_e is electromagnetic torque, U_q is the q-axis component of stator voltage, φ_f is the permanent magnet flux, P_n is the pole pairs, i_q is the q-axis equivalent component of stator current, L_q is the q-axis equivalent inductance of stator inductance, K_e is the back emf coefficient, R_s is the stator resistance, ω_e is the rotor angular velocity, T_L is the load torque, J_L is the equivalent rotational inertia, B_m is the damping coefficient, and ω_m is the mechanical angular velocity.

2.2.2. Axial piston pump model

Considering the compression and leakage of the axial piston pump, Eq. (2) displays the pump's intake and exit flow:

$$\begin{cases} q_1 = D_p \cdot n_p - C_{ip} \sqrt{p_1 - p_2} - C_{ep} \sqrt{p_1 - p_0} - V_1 \dot{p}_1 / \beta_c \\ q_2 = D_p \cdot n_p - C_{ip} \sqrt{p_1 - p_2} + C_{ep} \sqrt{p_2 - p_0} + V_2 \dot{p}_2 / \beta_c \end{cases} \quad (2)$$

where q_1 and q_2 represent the pump's intake and exit flow, p_1 , p_2 and p_0 represent the pump's high-pressure, low-pressure sides and oil discharge pressures, n_p is the pump speed, D_p is the pump displacement, C_{ip} and C_{ep} represent the pump's internal and external leakage coefficients, V_1 and V_2 are the pump's outlet and inlet sides compressed volume, and β_e is the oil's effective bulk modulus.

2.2.3. Straight through one-way cone valve model

The one-way valve can achieve one-way flow of oil. Due to the presence of viscous damping, there is a certain pressure drop when the oil passes through the one-way valve. Eq. (3) represents the interrelation between flow and pressure difference:

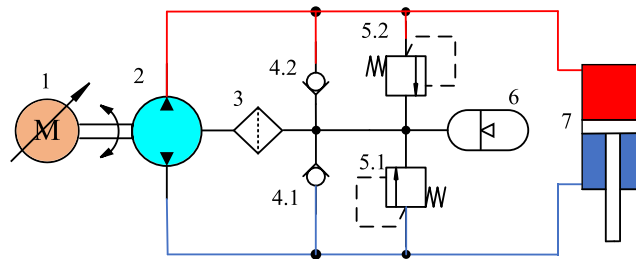
$$q_c = \Delta p_e^{\frac{1}{0.2p_k - 0.2}} = (p_a - p_0)^{\frac{1}{0.2p_k - 0.2}} \quad (3)$$

where q_c is the flow of the one-way valve, Δp_e is the one-way valve's pressure difference, p_a is the accumulator's outlet pressure, and p_k is the one-way valve's opening pressure.

2.2.4. Single rod piston hydraulic cylinder model

Engineering machinery usually uses a single rod piston hydraulic cylinder as the actuator, ignoring coulomb friction and disturbance force. The mathematical model can be shown as Eq. (4):

$$\begin{cases} q_L = A_c \dot{x}_c + C_{ic} p_L + V_i \dot{p}_L / (4\beta_c) \\ A_c p_L = m_c \ddot{x}_c + B_c \dot{x}_c + K x_c + F_{EL} \end{cases} \quad (4)$$



1: Servo motor; 2: axial quantitative piston pump; 3: Oil drain filter; 4.1/4.2: One-way valve; 5.1/5.2: Relief valve; 6: Accumulator; 8: cylinder

Fig. 1. Composition and working principle of the EHSPCS. 1: Servo motor; 2: axial quantitative piston pump; 3: Oil drain filter; 4.1/4.2: One-way valve; 5.1/5.2: Relief valve; 6: Accumulator; 8: cylinder.

where q_L is the load flow, A_c is the cylinder's effective working area, x_c is the piston rod displacement, C_{tc} is the total leakage coefficient of cylinder, V_t is the total compressed volume, p_L is the load pressure, m_c is the converted load's total mass, B_c is the viscous damping coefficient for the piston and load, K is the spring stiffness at load equivalent, and F_{EL} is external force acting as a load on the piston.

2.2.5. Oil drain filter model

To prevent scratches and blockages on pump, valves, and cylinder in the system, an oil drain filter needs to be placed. The interrelation between pressure difference, flow and flow area of the filter passage of the filter is expressed as Eq. (5):

$$Q_f = C_d K_A A_{f0} \sqrt{2(p_{f1} - p_{f2}) / \rho} \quad (5)$$

where Q_f is the filter's output flow, C_d is the flow coefficient, K_A is the effective area coefficient, A_{f0} is the initial filtration area, p_{f1} and p_{f2} are the filter's inlet and outlet pressures, and ρ is the oil's density.

Based on the hydraulic schematic diagram and mathematical models of various key components mentioned above, a simulation model of the EHSPCS is built using MATLAB/Simulink software for determining the system performance index threshold, algorithm design, and parameter debugging.

3. Establishment of the health assessment performance system for the EHSPCS

3.1. Analysis of factors influencing health assessment performance

The main task of establishing a health assessment performance indicator system is to determine performance indicators. Taking into account the factors that affect the operational status of the EHSPCS, this paper analyzes the three aspects of transmission medium, power input, and system efficiency to determine the performance indicators for system health assessment.

3.1.1. Analysis of hydraulic oil compressibility

Hydraulic oil, as the power transmission medium of the system, is a key factor to ensure stable output of the system. Oil compressibility is a major performance indicator of hydraulic oil, often characterized by the effective volume elastic modulus E , as shown in Eq. (6):

$$E = -V \left(\frac{dp}{dV} \right) \quad (6)$$

where p is the oil's working pressure, and V is the oil's volume.

The effective volume elastic modulus is mainly affected by the oil's working pressure, temperature, and gas content, and its relationship can be simplified as Eq. (7):

$$E = E_{sap} - m\Delta p + n\Delta T \quad (7)$$

where E_{sap} is the volume elastic modulus at standard atmospheric pressure, m is the pressure change coefficient of volume elastic modulus, Δp is the pressure change, n is the volume elastic modulus's temperature change coefficient. and ΔT is the temperature change.

When the system is in a steady-state state, the steady-state value f_{gH} of air mass void fraction set according to Herry's law is directly proportional to the oil pressure. The steady-state mathematical model for a given air mass void fraction can be expressed as Eq. (8) [23]:

$$f_{gH} = \begin{cases} f_g & (p \leq p_v) \\ f_{g0} \left(1 - \frac{p - p_v}{p_s - p_v} \right) & (p_v < p \leq p_s) \\ 0 & (p > p_s) \end{cases} \quad (8)$$

where f_{g0} is the initial amount of air in the oil, p_v is the liquid phase saturated vapor pressure, and p_s is the air separation pressure.

Typically, the volume elastic modulus of pure oil does not change much with pressure and temperature, while the oil's gas content has a significant impact on the volume elastic modulus. One of the major variables affecting system performance is the effective volume elastic modulus of the oil, which falls as the gas content rises.

3.1.2. Analysis of torque features of servo motor

As the power source of the EHSPCS, servo motor is the foundation for ensuring the establishment of system pressure and the output of actuator force. Eq. (9) displays the servo motor's output torque:

$$T_L = T_c - T_f - J_L \frac{d\omega_m}{dt} + B_m \omega_m \quad (9)$$

According to Eq. (9), without considering the mechanical losses of the motor ($T_f = 0$), The motor's load torque T_e is determined by the electromagnetic torque T_{em} of the motor. According to the Maxwell stress tensor method, T_{em} can be obtained as shown in Eq. (10) [24]:

$$T_{em} = \frac{2P_n l_{ef}}{\mu_0} \int_l r^2 B_n(\theta) B_\tau(\theta) d\theta \tag{10}$$

where T_{emT} is the theoretical electromagnetic torque, l_{ef} is the iron core's axial length, μ_0 is the vacuum permeability, r is the pole diameter at any point on the integral curve, $B_n(\theta)$ and $B_\tau(\theta)$ represent the normal and normal components of the air-gap flux density.

A motor's operating characteristics are significantly influenced by the air-gap density of the motor. The air-gap flux density's harmonic componen can cause an increase in electromagnetic torque fluctuation and vibration of the motor, affecting the smoothness of the motor's output torque [25].

3.1.3. Analysis of system leakage

System oil leakage is the main reason for system low efficiency and slow pressure building and regulation. The axial piston pump and the single rod piston hydraulic cylinder are the two primary components of the system that leak in this article. The leakage of axial piston pump is divided into gap leakage Q_{ldp} between the cylinder block and valve plate, gap leakage Q_{lp} between the piston and the inner wall of the cylinder body, and leakage Q_{isp} between the ball joint pair composed of the sliding shoe and the plunger. The total leakage Q_{tlp} can be expressed as Eq. (11) [26]:

$$Q_{tlp} = Q_{ldp} + Q_{lp} + Q_{isp} = \frac{\varphi_d r_d \delta_d^3}{12\mu l_d} p_1 + \frac{\pi d_p \delta_p^3 (1 + 1.5e_p^2)}{12\mu} \sum_{i=1}^n \frac{p_{cpi}}{L_{pi}} + \frac{\pi \delta_s^3}{6\mu \ln(r_2/r_1)} \sum_{i=1}^n p_{cpi} \tag{11}$$

where φ_d is the leakage angle of the oil allocating pair, r_d is the radius of the flow distribution shaft, δ_d is the gap between the rotor and plunger, μ is the oil dynamic viscosity, l_d is the contact length, d_p is the plunger diameter, δ_p is the oil clearance of the plunger pair, e_p is the eccentricity of the plunger, p_{cp} is the pressure difference between the low and high pressure chambers, L_p is the length of the contact surface between the cylinder block and plunger, δ_s is the slipper pair's oil clearance, r_1 and r_2 are the slipper pair oil sealing belt's inner and outer radius.

The leakage Q_{cl} of cylinders mainly occurs in the annular gap between the piston and cylinder body, which can be expressed as Eq. (12):

$$Q_{cl} = \frac{\pi d_c h_c^3}{12\mu l_c} \Delta p_c \pm \frac{v_c}{2} \pi d_c h_c \tag{12}$$

where d_c is the hydraulic cylinder piston diameter, v_c is the speed of the piston rod, h_c and l_c respectively represent the height and length of the clearance between the piston and the cylinder barrel's inner wall. When the speed direction is consistent with the pressure difference direction, "+" is taken, and vice versa, "-" is taken.

According to Eqs. (11) and (12), the system is affected by load pressure, which further affects the flow output and stable operation of the system. The system leakage coefficient can be used to characterize the size of the system leakage and reflect the operating status of the EHSPCS.

3.2. Establishment of health assessment performance indicators

Based on the analysis of factors affecting health assessment performance, this article takes the oil volume gas content, servo motor air-gap flux density, and system leakage coefficient as system health assessment performance indicators, and combines engineering practice to provide performance indicator thresholds for identifying the system in health, degradation, and failure states. The range of

Table 1
Parameters table of the EHSPCS.

Physical quantity	Symbol	Value	Unit
Cylinder's effective working area	A_c	71	mm ²
Total compressed volume	V_t	900	mL
Total mass of converted load	m_c	2000	kg
Pump displacement	D_p	1.5	mL/r
Viscous damping coefficient	B_c	150	N/(m/s)
Pump's internal leakage coefficient	C_{lp}	1×10^{-13}	(m ³ /s)/Pa
Pump's external leakage coefficient	C_{ep}	1×10^{-13}	(m ³ /s)/Pa
Cylinder's total leakage coefficient	C_{tc}	1×10^{-13}	(m ³ /s)/Pa
Effective volume elastic modulus	β_e	6.5×10^8	Pa
Load equivalent spring stiffness	K	9×10^7	N/m
Accumulator initial gas volume	V_{c0}	200	mL
Accumulator initial pressure	p_{c0}	3	MPa
Accumulator initial oil volume	V_0	200	mL

performance indicators for health assessment of the EHSPCS proposed in this article is derived from the Pump Control Oil Servomotor Fund project. It is required that the maximum overshoot of the system pressure should not exceed 0.5 MPa and the error at steady-state should not exceed 0.2 MPa when the input step pressure signal of the EHSPCS is 0–14 MPa. When the maximum overshoot of the system pressure is greater than 1 MPa or the steady-state error exceeds 0.5 MPa, it will cause damage to other equipment, and it is considered that the hydraulic system unable continue working. In addition, when the pressure on the suction side of the hydraulic pump is less than 0.1 MPa, it is also considered that the system is in a faulty state.

A single variable pressure step response simulation experiment was conducted using the established EHSPCS simulation experimental platform. The system parameters are shown in Table 1. Further compare the maximum overshoot and steady-state error of the system output pressure with the project requirements, and determine the performance threshold of the system under failure, degradation, and failure states as shown in Table 2:

4. Health assessment of LGA deep neural network for the EHSPCS

The health assessment methods for hydraulic systems are divided into two types: methods based on failure physical models and data-driven assessment methods. Considering the difficulty in obtaining accurate failure physical models for EHSPCS, and the fact that the EHSPCS can accumulate a large amount of state data reflecting the system's operating status during testing and use, this provides a data foundation for implementing data-driven health status assessment methods. This article proposes an LSTM-GRNN-ANN (LGA) deep neural network health assessment method that integrates LSTM, GRNN, and ANN (BP).

4.1. Principles of LGA deep neural network

The LGA deep neural network model consists of LSTM, GRNN, and ANN (BP), as seen in Fig. 2. The LSTM is applied to extract the features of temporal data in the time dimension; while the GRNN is applied to extract features of data in spatial dimensions. The ANN (BP) extracts feature and performance parameters fitting section, which is used to fit the nonlinear relationship between the extracted temporal and spatial data features and performance parameters. Compared to a single neural network, LGA neural network can capture the mutual influence between feature parameters and performance parameters from both temporal and spatial dimensions, which can improve the accuracy of health assessment models.

The input for LGA deep neural network model in Fig. 2 is the feature parameter values, and the output is the performance indicators. Time-series data is the feature parameter values arranged in chronological order by the EHSPCS. The “ y_1 ” output from the LSTM, the “ y_2 ” output from the GRNN, and the “ Y ” output from the ANN (BP) are all individual values, which are performance indicators values.

4.2. Extraction of feature parameters for LGA health assessment model

The health assessment model needs to select feature parameters as inputs, and further extract the temporal and spatial features of the system through LSTM and GRNN, respectively. The extraction process of feature parameters is as follows:

- (1) Feature parameters extraction of the oil volume gas content: The compressibility of oil is influenced by factors such as the volume change ΔV of the oil, the pressure change Δp of the oil, the temperature change ΔT of the system, and the oil volume gas content. Among them, oil volume gas content has the greatest impact on the compressibility of the oil, but it is difficult to directly measure and interacts with other factors that affect the compressibility of the oil, Therefore, neural network can be used to predict the oil volume gas content by using the directly measured variables mentioned above.
- (2) Feature parameters extraction of the motor air-gap flux density: Servo motor's air-gap flux density is influenced by factors such as controller output voltage U , motor q-axis current i_q , and motor operating temperature T . However, the air-gap flux density cannot be directly measured. Therefore, neural network can be available to predict the air-gap flux density using the directly measured variables mentioned above.
- (3) Feature parameters extraction of the system leakage: The leakage of system is primarily affected by factors such as the inlet pressure p_1 of pump, the outlet pressure p_2 , and the speed n_p of axial piston pump, but it is difficult to directly measure. Therefore, neural network are used to predict system leakage using the directly measured variables mentioned above. These variables can be collected through corresponding sensors on the testing platform, and the extracted feature parameters are shown in Table 3.

Table 2
Performance assessment threshold.

Health status	Oil volume gas content	Air-gap flux density (T)	Leakage coefficient
Health	< 8%	> 1.75	< 1.3
Degradation	8%–15%	1.75–1	1.3–5
Failure	≥15%	≤1	≥5

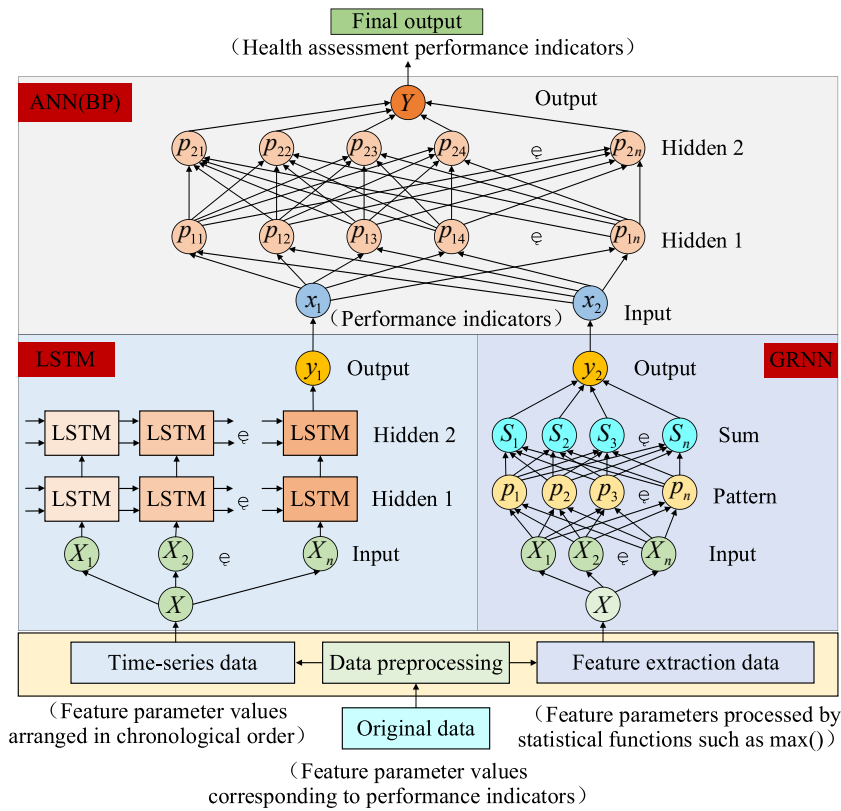


Fig. 2. Principle of LGA deep neural network model.

4.3. Design of system health assessment model

The health assessment model of the EHSPCS evaluates the degradation level based on health assessment performance indicators. The collected feature data is used as the original dataset of the model, with a portion of the dataset used as the training dataset to train the health evaluation model of the EHSPCS, and the other portion used as the testing dataset to test the accuracy of the health model evaluation. Three performance indicators correspond to one LGA neural network observer, and each LGA neural network observer corresponds to one LGA deep neural network. The structural principle of its model is shown in Fig. 3.

The input of the LGA observer is the feature parameter values, and the output is the performance indicators. The corresponding relationship between the two is shown in Table 3. The specific instructions for the input and output quantities of each LGA observer are

Table 3
Feature parameters of LGA health assessment model.

Performance indicators	Serial number	Feature parameter	Symbol	Unit
Oil volume gas content	1.1	Outlet pressure of pump	p_1	bar
	1.2	Rotational speed of pump	n_p	r/min
	1.3	Oil temperature	T	K
	1.4	Inlet pressure of hydraulic cylinder	p_3	bar
	1.5	Load torque of servo motor	T_L	N · m
Air-gap flux density of servo motor	2.1	Rotational speed of pump	n_p	r/min
	2.2	Operation temperature of servo motor	T_2	K
	2.3	Controller outputs control signals	U_e	mV
	2.4	q-axis current of servo motor	i_q	mA
	2.5	Output torque of servo motor	T_e	N · m
	2.6	Load torque of servo motor	T_L	N · m
System leakage coefficient	3.1	Rotational speed of pump	n_p	r/min
	3.2	Outlet pressure of pump	p_1	bar
	3.3	Inlet pressure of pump	p_2	bar
	3.4	Inlet pressure of hydraulic cylinder	p_3	bar
	3.5	Outlet pressure of hydraulic cylinder	p_4	bar
	3.6	Outlet flow of pump	q_1	L/min
	3.7	Inlet flow of pump	q_2	L/min

as follows:

- (1) The input of LGA observer 1 is the feature parameter values corresponding to the oil volume gas content, and the output is the oil volume gas content;
- (2) The input of LGA observer 2 is the feature parameter values corresponding to servo motor's air-gap flux density, and the output is the servo motor's air-gap flux density;
- (3) The input of LGA observer 3 is the feature parameter values corresponding to the system leakage coefficient, and the output is the system leakage coefficient.

According to the performance indicator threshold in Table 2, set the health status classification label of the system as shown in Table 4. The output results of system health performance indicators of LGA observers in Table 4 are indexed to obtain the overall health status of the EHSPCS.

4.4. Algorithm design and parameter debugging of LGA deep neural network

The algorithm design of the health assessment model in this article is founded on the MATLAB software's built-in neural network toolbox. The health assessment model is designed through parameter debugging of the invoked neural network function model through simulation. Collect 300 sets of state quantity data for each performance indicator of the system in both healthy and degradation states on the experimental platform, and 400 sets of state quantity data in fault state, totaling 3000 sets. Import the raw data into the MATLAB workspace in chronological order, divide the raw data into training and testing datasets, and standardize the data for algorithm design and parameter debugging.

4.4.1. GRNN module

The standardized data in the MATLAB workspace is processed by invoking the maximum function $\max()$, minimum function $\min()$, mean function $\text{mean}()$, and mean square error function $\text{var}()$ to obtain the feature matrix of the GRNN. Select the submatrix of the feature matrix as the network input, create a GRNN, and configure parameters. The number of neurons in the pattern layer and the summation layer is determined by the quantum particle swarm optimization algorithm, and the output layer is connected to the input layer of the ANN (BP) model.

The feature selection of GRNN has a significant impact on the accuracy of health assessment. In order to analyze the impact of each feature combination on the model evaluation results, different feature combinations were input into the model for training. The average prediction accuracy is obtained through the test, and the input feature group of the observer corresponding to the highest accuracy is selected as the input matrix of the GRNN module in each LGA observer to improve the accuracy of the overall health assessment results.

The feature selection of GRNN has a significant impact on the accuracy of health assessment. In order to analyze the influence of each feature combination on the model assessment results, different feature combinations are input to the model for training, and the average prediction accuracy is obtained through the test, and the observer input feature group corresponding to the highest assessment accuracy of the model is selected, and it is used as the input matrix of the GRNN module in each LGA observer to improve the overall accuracy of health assessment results.

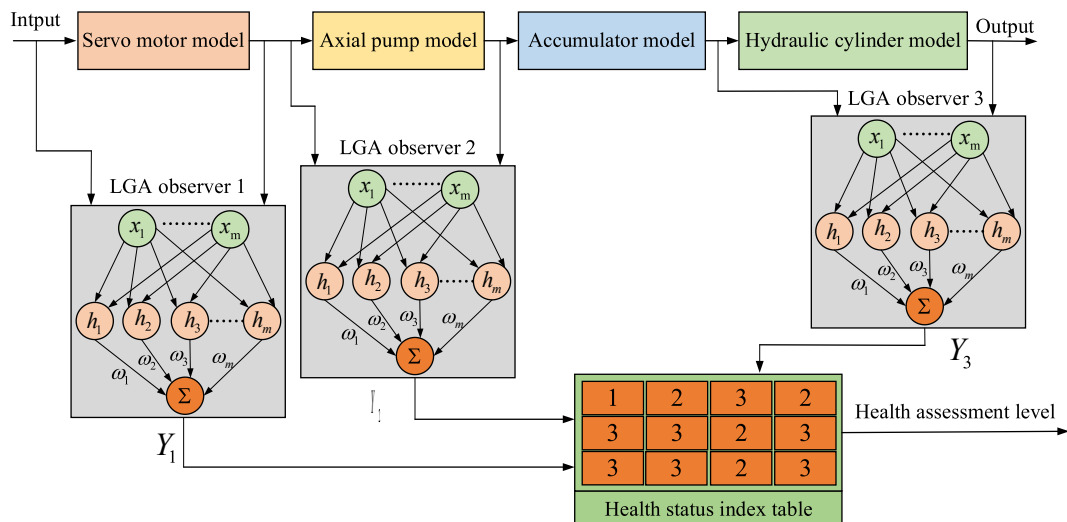


Fig. 3. Health assessment model of the EHSPCS.

Table 4
Feature parameters for LGA health assessment model.

Oil volume gas content	Air-gap flux density of servo motor	System leakage coefficient	Label
H	H	H	1
H	H	D	2
H	H	F	3
H	D	H	2
H	D	D	2
H	D	F	3
H	F	H	3
H	F	D	3
H	F	F	3
D	H	H	2
D	H	D	2
D	H	F	3
D	D	H	2
D	D	D	2
D	D	F	3
D	F	H	3
D	F	D	3
D	F	F	3
F	H	H	3
F	H	D	3
F	H	F	3
F	D	H	3
F	D	D	3
F	D	F	3
F	F	H	3
F	F	D	3
F	F	F	3

Note: H represents health, D represents degradation, and F represents failure.

4.4.2. LSTM module

Compose the standardized data in the MATLAB workspace into an input matrix in chronological order, create an LSTM, and configure parameters. The network consists of two hidden layers, connected by Dropout to prevent overfitting, and the output is constrained by ReLU activation function. The output layer consists of a fully connected layer and a softmax layer, which are connected to the input layer of the ANN. The network optimizer is Adam.

The learning rate and batch processing volume of the main hyperparameters of the LSTM have a significant impact on the accuracy of the assessment results. To analyze the impact of each hyperparameter on the model, the single variable principle is adopted. During each training, only one variable's value is changed, and other variables are fixed for simulation experiments. The results are shown in Fig. 4.

From Fig. 4A, the assessment accuracy shows a trend of first increasing and then decreasing as the number of learning rates increases. When the learning rate is 0.01, the assessment accuracy of the model is the highest, so 0.01 is set as the learning rate during the training process; From Fig. 4B, the assessment accuracy tends to decrease as the batch processing volume increases. When the batch size is 16, the assessment accuracy of the model is the highest. Therefore, 0.01 and 16 are set as the learning rate and maximum batch processing during the training process, respectively. The hyperparameter values of other LSTM are shown in Table 5.

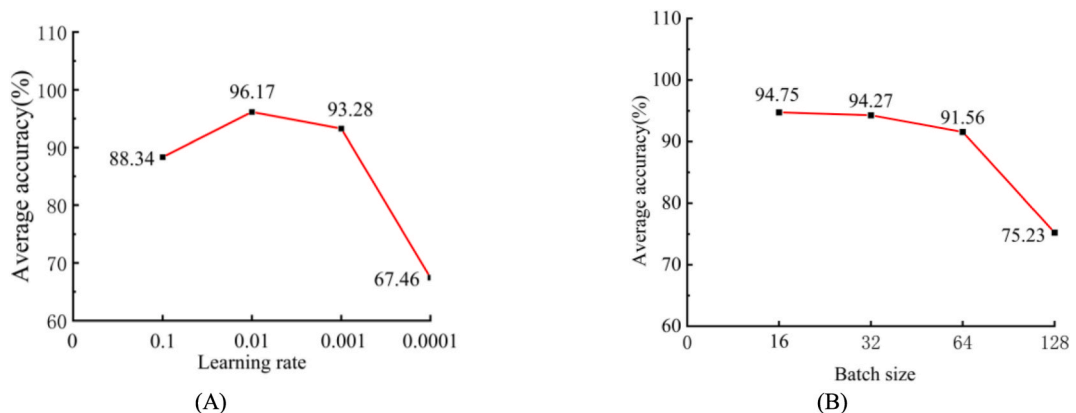


Fig. 4. Assessment accuracy under different learning rates and batch processing volumes. Figure A: Assessment accuracy for different learning rates; Figure B: Assessment accuracy of different batch processing volumes.

4.4.3. ANN(BP)module

The input matrix X of the ANN (BP) is obtained by combining the outputs of LSTM and GRNN. The ANN's (BP) structure is as follows:

The input layer has two neurons for inputting the outputs of GRNN and LSTM.

The output layer has one neuron for outputting performance parameters.

There are two hidden layers in the middle, where each hidden layer's total number of neurons is determined by the improved quantum particle swarm optimization (QPSO) algorithm.

4.4.4. QPSO algorithm

The QPSO algorithm is based on swarm optimization algorithms to find the optimum for the target task, where particles represent a feasible solution. This article uses QPSO to maximize the number of neurons in two hidden layers of a neural network. The range of values for each hidden layer's number of neurons is [5500]. The goal task is to accurately predict the performance indicators values, and the calculation process is shown in Fig. 5.

5. Design of performance indicators test

5.1. Test platform

A test platform for the (steam turbine) pump control servomotor was built as shown in Fig. 6. Through functional valve blocks, the servo motor, axial piston pump, hydraulic valves, and sensor are incorporated into the cylinder. The mechanical spring is connected to the cylinder by a abutment to simulate the load, and necessary electrical components including the shaft controller and servo driver are integrated within the electric control cabinet [7].

The main component models of the hydraulic system are shown in Table 6.

The experimental platform is equipped with torque, flow, pressure, and temperature sensors for measuring torque, flow, pressure, and temperature signals in the feature parameters. Other feature parameters signals such as control signals, phase currents, and pump output speed can be directly read from the servo motor driver.

5.2. Design of experimental content

Based on the performance indicators analysis in the previous text, the hydraulic system of the pump control servomotor is modified, and oil gas content failure simulation test, servo motor air-gap eccentricity failure simulation test, and system oil leakage failure simulation test are designed for verifying the feasibility of the proposed a system health assessment method using LGA deep neural network.

5.2.1. Oil gas content failure simulation test

This article analogs an oil containing gas failure by connecting a valve block (3.1, 3.2) with different cavities in series between the axial piston pump and hydraulic cylinder. The outlet and inlet of the valve block are connected to the cylinder and pump through two sets of shut-off valves, as shown in Fig. 7.

It is necessary to complete the filling and exhaust of the system before the gas content simulation test. After the filling and venting operation, the oil's initial mass gas content in the system is about 8.05×10^{-6} , with a volumetric air content of about 3%. The air content control valve block is equipped with cavities of different volumes. The volumes of each cavity are calculated based on the air content of 4%, 6%, 8%, 10%, 12%, 14%, and 16%. During the test, open the shut-off valves at both ends of the corresponding cavities with different volumes in sequence for simulation testing. Download the program written by AutoThink software to the HollySys motion controller, use the software program to give the system a step pressure signal command of 0–14 MPa, and collect the system's state signal through sensors. After each test is completed, the system needs to be filling and venting operation.

5.2.2. Servo motor air-gap eccentricity failure simulation test

In practical work, servo motor are not only contaminated by dust and hydraulic fluid, but also have problems such as structural wear, strong electromagnetic interference, and load impact, which makes the motor prone to failure during operation. Among them, the thermal effect of the stator winding phase current of the servo motor will cause copper loss in the stator winding, which will reduce the air gap magnetic density of the motor, thus affecting the low-speed characteristics and torque output of the motor. The occurrence of air-gap eccentricity failure in permanent magnet synchronous motors will increase the effective value of stator winding phase current and increase the copper loss of the winding.

This article designs a motor failure eccentricity test to validate the accuracy of the health assessment model in predicting

Table 5
Hyperparameters of LSTM.

Max Epochs	Dropout Layer	Learn Rate	Gradient Threshold	LearnRate DropPeriod	LearnRate DropFactor
16	0.1	0.01	0.9	125	0.2

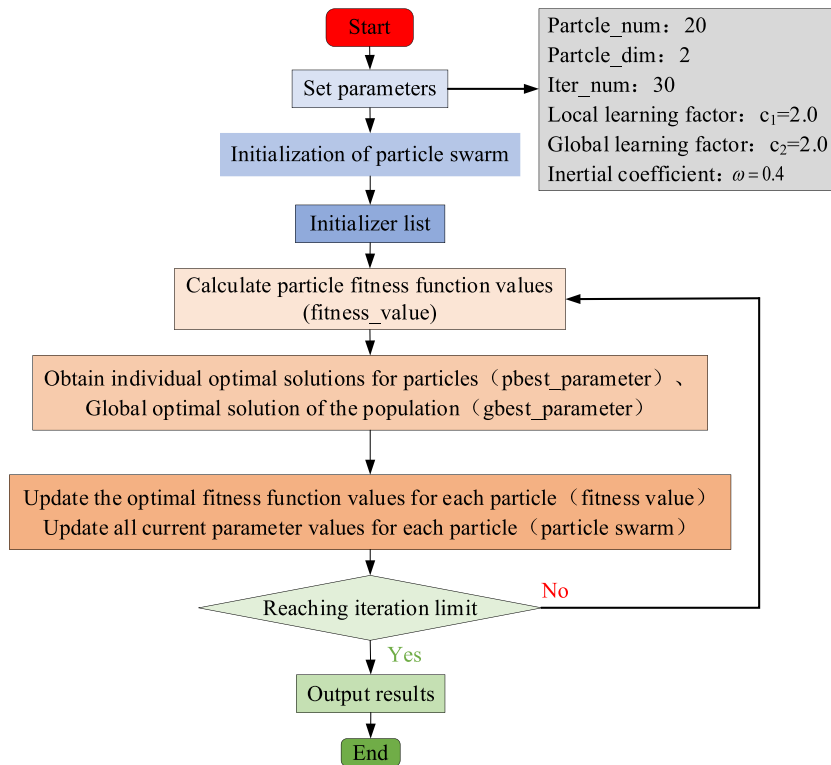


Fig. 5. Process of quantum particle Swarm optimization algorithm.

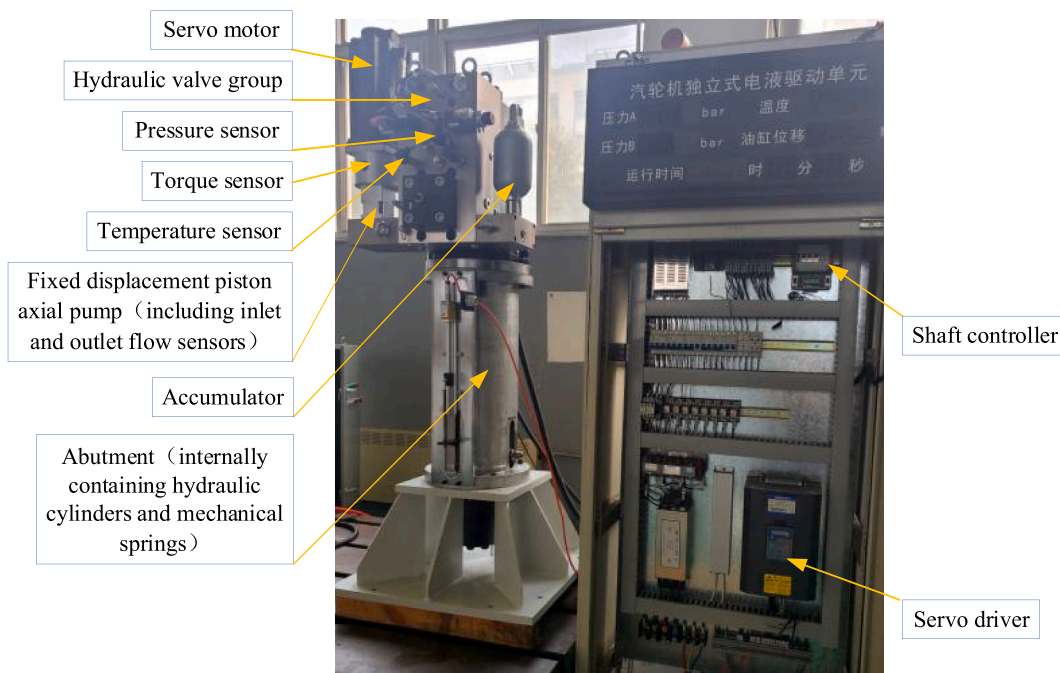


Fig. 6. Test platform for the pump control servomotor.

performance indicators such as air-gap flux density. However, due to limited experimental conditions, this article uses a controller to limit the voltage output to the synchronous motor to simulate motor static eccentricity failure. By software programming, the output pressure signals are limited to 95%, 93%, 91%, 89%, and 87% of the normal values. The program written by AutoThink software is

Table 6
Information on the primary hydraulic parts.

Serial number	Name	Model	Parameters
1	Servo motor	HP11321-G202A	Nominal torque: 23.5 N m Nominal speed: 3000 r/min
2	Axial piston pump	TFH-630-U-PCV-F	Displacement: 6.3 mL/r Nominal speed: 21 MPa
3	Accumulator	NXQ-A-2.5/31.5-L-Y	Nominal volume: 2.5 L Nominal pressure: 31.5 MPa
4	Pressure sensor	PR110-3403-17-C3.37	Measurement range: 0–25 MPa
5	Temperature sensor	STC-C0120-B04-420A-1-50-F	Measurement range: 0~ +120 °C

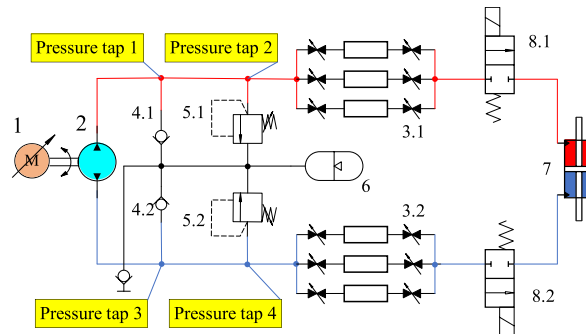


Fig. 7. Hydraulic schematic diagram for oil gas content simulation test.

downloaded to the HollySys motion controller, and the step pressure signal command of the system is given as 0–14 MPa using the software program. The state signal of the system is collected as training and testing sample data for the health assessment model.

5.2.3. System oil leakage failure simulation test

The pump and cylinder may experience abrasion and increase axial clearance during long-term use, which can cause partial oil to directly return to the suction chamber from the oil discharge port, making the system flow unable to reach the rated flow rate, resulting in the inability to maintain system pressure and an increase in pressure steady-state error.

This article uses electric-proportional throttle valves (9.1, 9.2) connected in series between the outlet and inlet ports of the cylinder and pump, respectively. By controlling the electric-proportional throttle valve opening to simulate different leakage faults in the system. Fig. 8 displays the experiment’s schematic diagram of the hydraulic system.

By analyzing the sample of electronic-proportional throttle valve sample, the flow pressure drop curves of 11 throttle valves with different throttle opening degrees were selected, and the corresponding leakage coefficient was calculated as the expected performance indicator. The specific operating steps for the system leakage simulation test are:

- (1) Follow the filling and venting operation steps in the oil gas content simulation test until there are no obvious bubbles in the oil flowing out of the reserved pressure measuring point;
- (2) Adjust the opening of the electric-proportional throttle valves to the preset position 2, download the AutoThink software program to the HollySys motion controller, and use the software program to give the system a step pressure signal command of 0–14 MPa. When the system pressure remains a steady state, the system state signals are collected as training and testing sample data for the health assessment model;

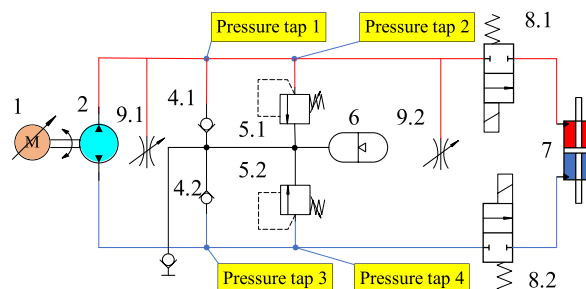


Fig. 8. Hydraulic schematic diagram for system oil leakage failure simulation test.

- (3) Respectively control the electric-proportional throttle valves to adjust the size of the throttle port to the preset positions 3, 4, 5, 6, 7, 8, 9, 10, 11, 11.5, and repeat the previous operation;
- (4) Import the collected sample data into the MATLAB workspace for subsequent processing and application of the sample data.

6. Experimental testing and result analysis

6.1. Signal data preprocessing

The working environment of EHSPCS in practical engineering applications is relatively harsh, usually with strong electromagnetic interference and circuit thermal noise. The electrical components used in the measurement system state sensor are more sensitive, and the output signal will inevitably be interfered, resulting in low or even unusable signal measurement accuracy. The health assessment model of the EHSPCS is a data-driven model. The collected signals of the EHSPCS state variables have a significant impact on the evaluation results, and noise signals may cause the model assessment results to be inconsistent with the actual state of the system, resulting in “false alarms”. Therefore, it is necessary to denoise the collected signals.

Kalman filter is the optimal state estimator for linear Gaussian space models. It improves the accuracy of signal estimation by using dynamic systems containing uncertain factors, and is widely used in the field of health assessment. However, inaccurate prior information can cause an increase in Kalman filter estimation error and even filter divergence. The adaptive Kalman filter based on the IMM algorithm estimates the current state and covariance by setting a model set containing multiple motion states, and fusing the estimated values and covariance matrices between different model sets, thereby reducing estimation errors and avoiding filtering signal divergence. Therefore, this article uses an adaptive Kalman filter based on the IMM algorithm to filter the collected signals [27]. Filter and process the collected system pressure signal using an IMM adaptive filter in MATLAB.

6.2. Experimental testing analysis

The failure simulation test is conducted on the established test platform, collecting the state signals of the system under health, degradation, and failure during the failure simulation test, and processing them through an IMM adaptive filter as the dataset for training and testing the model.

The oil gas content failure simulation test collects 300 sets of health and degradation status data for each system, and 400 sets of failure status data, totaling 1000 sets. 700 sets of data are randomly select as the training dataset for the model, and the remaining 300 sets of data regard as the testing. By substituting the above data into the LGA deep neural network model for analysis, the health assessment results and health assessment error of oil gas content are shown in Fig. 9A and B, respectively.

The servo motor air-gap eccentricity failure simulation test collected 300 sets of system health and degradation status data each, and 400 sets of failure status data, totaling 1000 sets. 700 sets of data are randomly select as the training dataset for the model, and the remaining 300 sets of data regard as the testing dataset for the model. By substituting the above data into the LGA deep neural network model for analysis, the health assessment results and health assessment error of air-gap flux density are shown in Fig. 10A and B, respectively.

The system leakage failure simulation test collected 300 sets of system health status and degradation status data, and 400 sets of failure status data, totaling 1000 sets. 700 sets of data are randomly select as the training dataset for the model, and the remaining 300 sets of data regards the testing. By substituting the above data into the LGA deep neural network model for analysis, the health assessment results and health assessment error of the system leakage coefficient are shown in Fig. 11A and B, respectively.

From Figs. 9–11, it can be seen that the error between the assessment value of oil gas content and the theoretical value is less than 5×10^{-3} , the error between the assessment air-gap flux density value and the theoretical value is less than 5×10^{-2} , the error between the assessment value of the system leakage coefficient and the theoretical value is less than 0.02.

The prediction results are indexed into the system health table to obtain the health assessment results of the LGA deep neural network as shown in Fig. 12C and compared with the assessment results of the LSTM shown in Fig. 12A and the GRNN shown in Fig. 12B. The results are shown in Fig. 12D.

From the above graph figure, it can be seen that the average accuracy of the LSTM health assessment model is 89.84%, the GRNN health assessment model average accuracy is 87.99%, and the average accuracy of LGA deep neural network health assessment model can reach up to 96.37%. The aforementioned findings indicate that the health assessment model suggested in this article can accurately evaluate the health status of the EHSPCS.

7. Conclusion

The health status assessment method of the EHSPCS for servomotor is investigated in this study. The variables influencing the operation's status of the EHSPCS are analyzed. With oil gas content, servo motor air-gap flux density, and system leakage coefficient as the system's health evaluation performance indicators, a health assessment performance indicators system of the system is established. The performance index thresholds of the system under health, degradation, and failure are set, and the feature parameters that affect the changes in performance indicators are given. Based on this, a health assessment method based on LSTM-GRNN-ANN (LGA) deep neural network is proposed. LSTM and GRNN are used to extract the feature parameters of performance indicators in both temporal and spatial dimensions, and ANN (BP) is used to fit the nonlinear relations between performance parameters and data features. The QPSO is used to optimize the parameters of the LGA deep neural network, and an LGA deep neural network-based health assessment

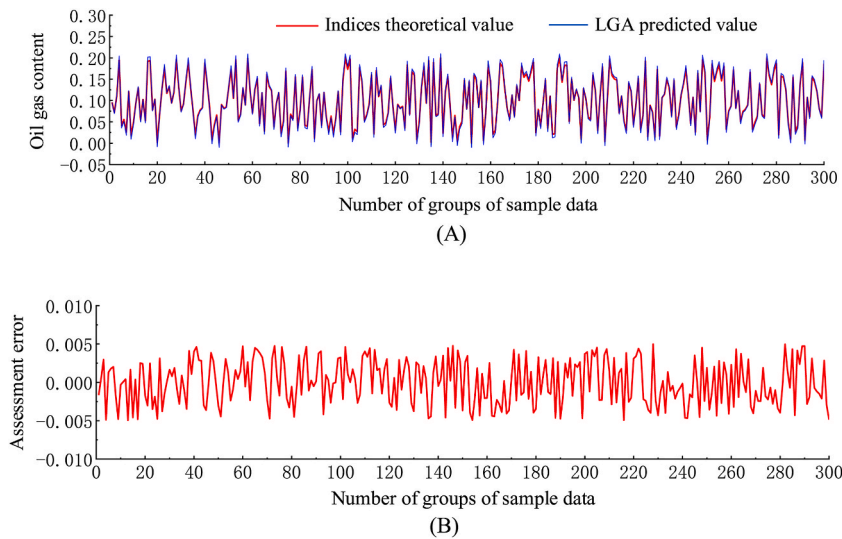


Fig. 9. Health assessment of oil gas content. Figure A: Health assessment results; Figure B: Health assessment error.

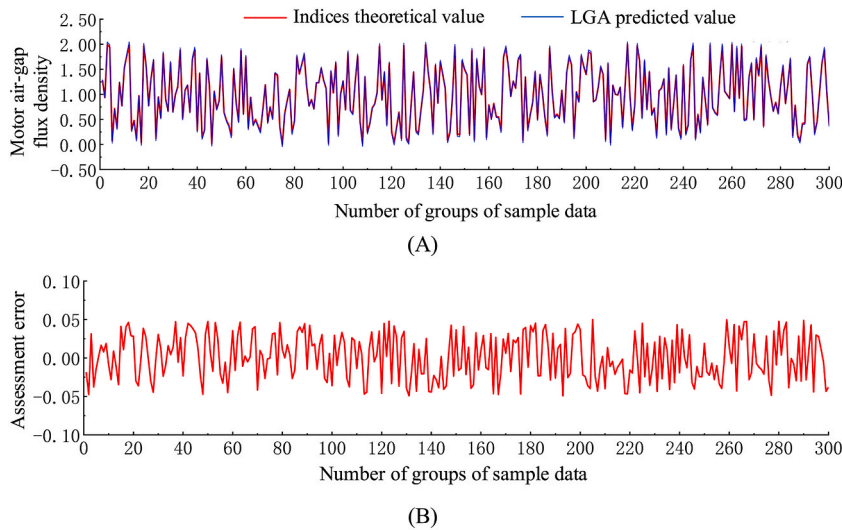


Fig. 10. Health assessment of air-gap flux density. Figure A: Health assessment results; Figure B: Health assessment error.

model for EHSPCS is established. Experimental testing shows that the health assessment model's average accuracy based on LGA deep neural network proposed in this article is 97.48%, which has higher accuracy compared to LSTM and GRNN evaluated separately. A theoretical and technical foundation for the dependable operation of EHSPCS will be provided by this study. The next step is to optimize the health indicator system and evaluation model of EHSPCS and attempt practical engineering applications. In addition, enhancing the intelligence of health assessment and improving the self-learning, self optimization, and adaptive capabilities of algorithms is of great significance for future work.

Ethics statement

Review and/or approval by an ethics committee was not needed for this study because the article focuses on engineering issues and does not involve ethical issues.

Funding statement

This work was supported by Science and Technology Research Project of Colleges and Universities of Hebei Province [No. ZD2021340].

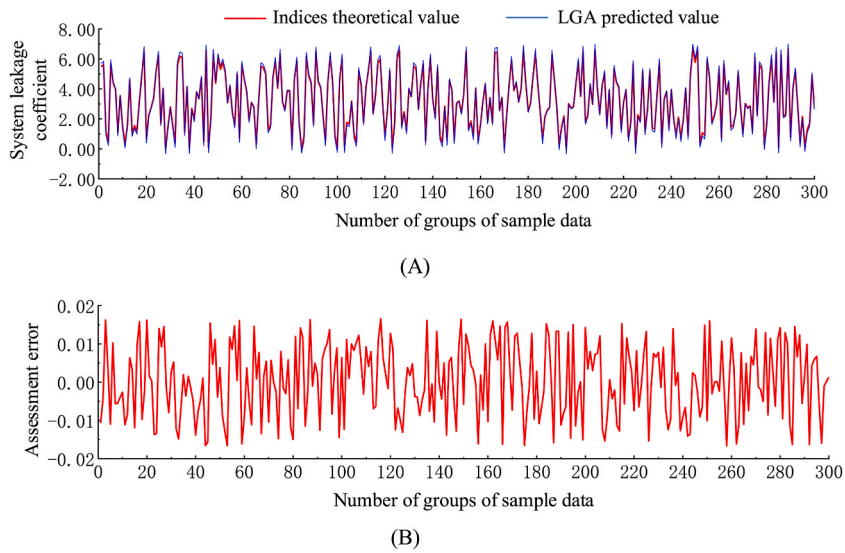


Fig. 11. Health assessment of the system leakage coefficient. Figure A: Health assessment results; Figure B: Health assessment error.

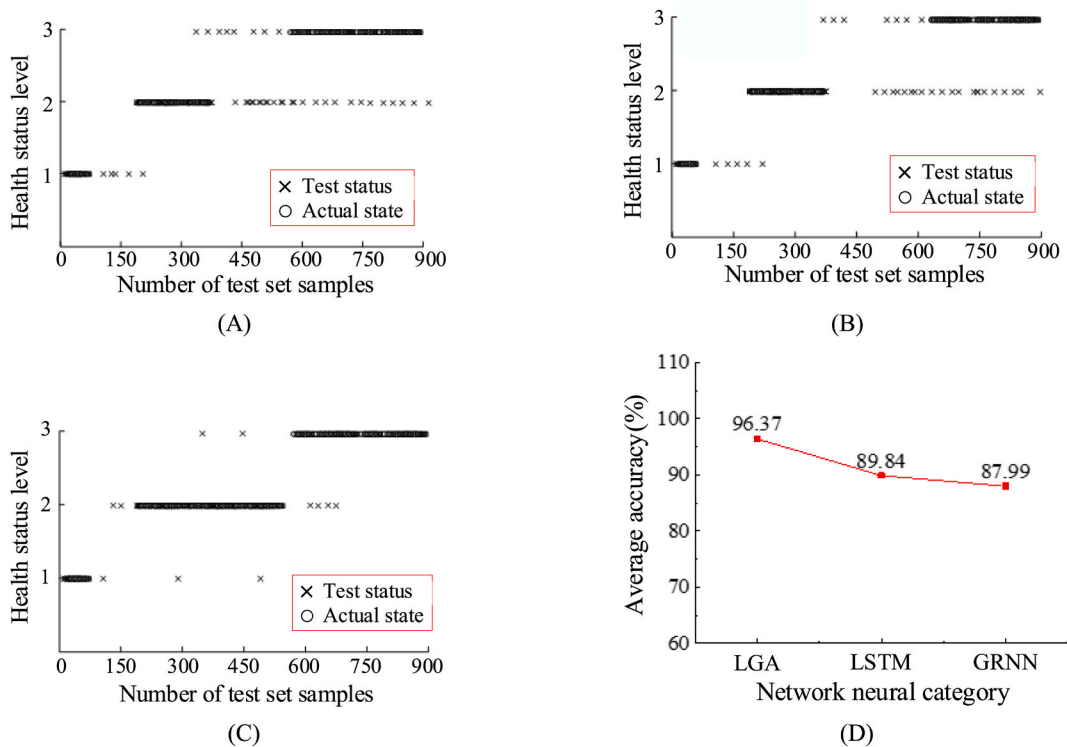


Fig. 12. Evaluation accuracy and comparison of different neural networks. Figure A: Health assessment results of LSTM; Figure B: Health assessment results of GRNN; Figure C: Health assessment results of LGA neural network; Figure D: Comparison of accuracy of different health assessment.

This work was supported by Natural Science Foundation of Xinjiang Uygur Autonomous Region [No. 2022D01A51].

Data availability statement

Data included in article/supp. material/referenced in article.

CRedit authorship contribution statement

Fei Wang: Data curation, Writing – original draft. **Gexin Chen:** Methodology, Project administration, Writing – review & editing. **Keyi Liu:** Formal analysis, Funding acquisition. **Tiangui Zhang:** Software, Validation. **Yuan Li:** Conceptualization, Investigation. **Chao Ai:** Data curation, Supervision, Writing – review & editing.

Declaration of competing interest

The authors declare that they have no known competing financial interests or personal relationships that could have appeared to influence the work reported in this paper.

References

- [1] K. Chen, R. Tang, C. Li, J. Lu, Fractional order PI^{λ} controller synthesis for steam turbine speed governing systems, *ISA Trans.* 77 (2018) 49–57, <https://doi.org/10.1016/j.isatra.2018.03.017>.
- [2] F. Wang, G. Chen, H. Liu, G. Yan, T. Zhang, K. Liu, Y. Liu, C. Ai, Research on position control of an electro-hydraulic servo closed pump control system, *Processes* 10 (9) (2022) 1674, <https://doi.org/10.3390/pr10091674>.
- [3] N. Alle, S.S. Hiremath, S. Makaram, K. Subramaniam, A. Talukdar, Review on electro hydrostatic actuator for flight control, *Int. J. Fluid Power* 17 (2) (2016) 125–145, <https://doi.org/10.1080/14399776.2016.1169743>.
- [4] C. Ai, L. Zhang, W. Gao, G. Yang, D. Wu, L. Chen, A. Plummer, A review of energy storage technologies in hydraulic wind turbines, *Energy Convers. Manag.* 264 (2022) 115584, <https://doi.org/10.1016/j.enconman.2022.115584>.
- [5] W. Shen, Y. Pang, J. Jiang, Robust controller design of the integrated direct drive volume control architecture for steering systems, *ISA Trans.* 78 (2018) 116–129, <https://doi.org/10.1016/j.isatra.2017.05.008>.
- [6] Z. Li, C. Wang, L. Quan, L. Ge, L. Xia, Study on energy efficiency features of the heavy-duty manipulator driven by electro-hydraulic hybrid active-passive system, *Autom. Construct.* 125 (7) (2021) 103646, <https://doi.org/10.1016/j.autcon.2021.103646>.
- [7] W. Hong, S. Wang, M.M. Tomovic, H. Liu, J. Shi, X. Wang, A Novel indicator for mechanical failure and life prediction based on debris monitoring, *IEEE Trans. Reliab.* 66 (1) (2016) 161–169, <https://doi.org/10.1109/TR.2016.2628412>.
- [8] M. Yang, G. Yan, Y. Zhang, T. Zhang, C. Ai, Research on high efficiency and high dynamic optimal matching of the electro-hydraulic servo pump control system based on NSGA-II, *Heliyon* 9 (3) (2023) 1, <https://doi.org/10.1016/j.heliyon.2023.e13805>.
- [9] G. Yan, Z. Jin, T. Zhang, C. Zhang, C. Ai, G. Chen, Exploring the essence of servo pump control, *Processes* 10 (4) (2022) 786, <https://doi.org/10.3390/pr10040786>.
- [10] Z. Ma, H. Liao, J. Gao, S. Nie, Y. Geng, Physics-informed machine learning for degradation modeling of an electro-hydrostatic actuator system, *Reliab. Eng. Syst. Saf.* 229 (2023) 108898, <https://doi.org/10.1016/j.res.2022.108898>.
- [11] P.A. Scandura, Integrated vehicle health management as a system engineering discipline, in: 24th Digital Avionics Systems Conference, Washington, DC, USA, vol. 2, 2005, p. 10, <https://doi.org/10.1109/DASC.2005.1563450>.
- [12] D. Kim, T.Y. Heo, Anomaly detection with feature extraction based on machine learning using hydraulic system IoT sensor data, *Sensors* 22 (7) (2022) 2479, <https://doi.org/10.3390/s22072479>.
- [13] F. Kosova, H.O. Unver, A digital twin framework for aircraft hydraulic systems failure detection using machine learning techniques, *Proc. Inst. Mech. Eng., C: J. Mech. Eng. Sci.* 237 (7) (2023) 1563–1580, <https://doi.org/10.1177/09544062221132697>.
- [14] A. Macaluso, G. Jacazio, Prognostic and health management system for fly-by-wire electro-hydraulic servo actuators for detection and tracking of actuator faults, *Procedia Cirp* 59 (2017) 116–121, <https://doi.org/10.1016/J.PROCIR.2016.09.016>.
- [15] S. Duan, Y. Li, Y. Cao, X. Wang, X. Li, Z. Zhao, Health assessment of landing gear retraction/extension hydraulic system based on improved risk coefficient and FCE model, *Appl. Sci.* 12 (11) (2022) 5409, <https://doi.org/10.3390/app12115409>.
- [16] S. Mei, M. Yuan, J. Cui, S. Dong, J. Zhao, Health condition assessment of hydraulic system based on cloud model and dempster–shafer evidence theory, in: *Advances in Precision Instruments and Optical Engineering: Proceedings of the International Conference on Precision Instruments and Optical Engineering, 2021*, Springer Nature Singapore, Singapore, 2022, pp. 567–577, https://doi.org/10.1007/978-981-16-7258-3_54.
- [17] A. Gareev, V. Protsenko, D. Stadnik, et al., Improved fault diagnosis in hydraulic systems with gated convolutional autoencoder and partially simulated data, *Sensors* 21 (13) (2021) 4410, <https://doi.org/10.3390/s21134410>.
- [18] K. Lu, Z. Wu, T. Huang, Differential evolution-based three stage dynamic cyber-attack of cyber-physical power systems, *IEEE ASME Trans. Mechatron.* 28 (2) (2022) 1137–1148, <https://doi.org/10.1109/TMECH.2022.3214314>.
- [19] M. Chen, G. Zeng, K. Lu, J. Weng, A two-layer nonlinear combination method for short-term wind speed prediction based on ELM, ENN, and LSTM, *IEEE Internet Things J.* 6 (4) (2019) 6997–7010, <https://doi.org/10.1109/JIOT.2019.2913176>.
- [20] A.T. Keleko, B. Kamsu-Foguem, R.H. Ngouna, A. Tongne, Health condition monitoring of a complex hydraulic system using deep neural network and DeepSHAP explainable XAI, *Adv. Eng. Software* 175 (10) (2023) 33–39, <https://doi.org/10.1016/j.advengsoft.2022.103339>.
- [21] D. Song, C. Lu, J. Ma, Y. Cheng, Health assessment for hydraulic system based on GRNN and metric learning, *IFAC-PapersOnLine* 53 (3) (2020) 37–42, <https://doi.org/10.1016/j.ifacol.2020.11.007>.
- [22] S. Nie, J. Gao, Z. Ma, F. Yin, H. Ji, An online data-driven approach for performance prediction of electro-hydrostatic actuator with thermal-hydraulic modeling, *Reliab. Eng. Syst. Saf.* 236 (2023) 109289, <https://doi.org/10.1016/j.res.2023.109289>.
- [23] X. Yuan, C. Wang, X. Zhu, L. Zhang, Research on theoretical model of dynamic bulk modulus of elasticity of gas-liquid mixed fluid, *Mech. Eng.* 56 (2020) 209–217, <https://doi.org/10.3901/JME.2020.04.209>.
- [24] Q. Ye, H. Lin, On deriving the Maxwell stress tensor method for calculating the optical force and torque on an object in harmonic electromagnetic fields, *Eur. J. Phys.* 38 (4) (2017) 045202, <https://doi.org/10.1088/1361-6404/aa6e1d>.
- [25] G. Zhao, Y. Zhang, H. Ge, Y. Liu, B. Bai, Prediction of flux density distribution in permanent magnet motor with eccentric magnetic pole, *Electr. Mach. Control* 24 (6) (2020) 24–32, <https://doi.org/10.15938/j.emc.2020.06.004>.
- [26] J.M. Bergada, S. Kumar, D.L. Davies, J. Watton, A complete analysis of axial piston pump leakage and output flow ripples, *Appl. Math. Model.* 36 (4) (2012) 1731–1751, <https://doi.org/10.1016/j.apm.2011.09.016>.
- [27] W. Lyu, X. Cheng, J. Wang, Adaptive federated IMM filter for AUV integrated navigation systems, *Sensors* 20 (23) (2020) 6806, <https://doi.org/10.3390/s20236806>.